metry. $T_{1\rho}$ measurements and observation of differential line broadening indicate that this internal motion has at least two components. One, with an approximately 7 kcal/mol activation energy, probably involves the disulfide bridge and adjacent groups. Another motion of much lower barrier probably involves rotation of amide planes relative to the average ring plane, with little change in $\alpha$-carbon positions. The latter motion is common to other cyclo(Ala-Gly-Pro-Phe)$_2$ analogues.

The exchange contributions to $T_{1\rho}$ relaxation in peptides reflect conformational mobility in the 1-100 $\mu$s range. Analysis of these contributions from complex conformation equilibria as though they arise from two-site exchanges gives reasonable indications of conformational lifetimes and site-to-site chemical shift differences.

**Acknowledgment.** This research was supported by grants from the National Institute of General Medical Sciences, GM 22490 (K.K.B) and GM 26071 (K.D.K.). Mass spectra were obtained by the Midwest Center for Mass Spectrometry at the University of Nebraska, a National Science Foundation Regional Instrumentation Facility (CHE 821164). We are indebted to Dr. Cynthia D'Ambrosio, Smith Kline and French Laboratories, for the 500-MHz spectra shown in Figure 4.

**Registry No.** BOC-Cys(Acm)-Gly-Pro-Phe-OMe, 114423-77-7; BOC-(Cys(Acm)-Gly-Pro-Phe)$_2$-NHNH$_2$, 114423-78-8; cyclo(Cys-(Acm)-Gly-Pro-Phe)$_2$, 114423-79-9; cyclo(Cys-Gly-Pro-Phe)$_2$, 111967-73-8; cyclo(Cys-Gly-Pro-Phe)$_2$·4H$_2$O, 114423-80-2; Cbz-Pro-ONSu, 3397-33-9; Cbz-Gly-ONSu, 2899-60-7; BOC-Cys(Acm)-ONSu, 19746-38-4; H-Phe-OMe, 2577-90-4; BOC-Cys(Acm)-Gly-Pro-Phe-NHNH$_2$, 114423-81-3; H-Cys(Acm)-Gly-Pro-Phe-OMe·HCl, 114423-82-4; BOC-(Cys(Acm)-Gly-Pro-Phe)$_2$-OMe, 114423-83-5; H-(Cys(Acm)-Gly-Pro-Phe)$_2$-NHNH$_2$·HCl, 114423-84-6; cyclo(Alu-Gly-Pro-Phe)$_2$, 91383-23-2.

**Supplementary Material Available:** Tables of atomic coordinates and thermal parameters for cyclo(Cys-Gly-Pro-Phe)$_2$·4H$_2$O (6 pages); listing of observed and calculated structure factors (19 pages). Ordering information is given on any current masthead page.

# $^1$H NMR Resonance Assignment and Dynamic Analysis of Phenylalanine CD1 in a Low-Spin Ferric Complex of Sperm Whale Myoglobin

**S. Donald Emerson, Juliette T. J. Lecomte,† and Gerd N. La Mar***

*Contribution from the Department of Chemistry, University of California, Davis, California 95616.* *Received September 28, 1987*

**Abstract:** A proton NMR investigation has been carried out to characterize the dynamic properties of the ring reorientation of the highly conserved phenylalanine CD1 of sperm whale myoglobin. The paramagnetic (Fe(III), $S = {}^1/_2$) met-cyano derivative imparts large chemical shift dispersion that allows detection of the rapid reorientation while retaining relatively narrow lines amenable to unambiguous assignment. The side chain ring peaks for Phe CD1 are assigned on the basis of steady-state and time-dependent nuclear Overhauser effect measurements among the side-chain resonances and between the side-chain resonances and heme resonances in both native and deuterohemin-reconstituted metMbCN and on the basis of differential paramagnetic relaxation. The quantitation of exchange contributions to the line width of the averaged meta H resonances of the ring as a function of temperature yields a ring reorientation rate of $\sim 10^5$ s$^{-1}$ at 25 °C and an activation barrier of 14 ± 4 kcal/mol. This barrier is consistent with a low activation energy process indicative of local concerted structural fluctuations of the C-D helical corner and is inconsistent with global unfolding. The highly conserved nature of the Phe CD1 and its characteristic hyperfine shift that places it in the resolved portion of the $^1$H NMR spectrum of met-cyano derivatives suggest that the rate of Phe CD1 ring rotation should serve as a useful probe of local dynamic properties of the CD corner in a variety of oxygen-binding heme proteins.

The functional properties of biopolymers are known to be determined not only by their ground-state structure, well described by crystal diffraction methods, but also by their dynamic fluctuations.[1-5] For the oxygen-binding heme proteins myoglobin, (Mb) and hemoglobin (Hb), the biologically important motions range from side-chain rotations that allow oxygen to permeate into the crowded heme pocket[6-8] to large segmental displacements that are involved in cooperativity.[9-11] The remarkable distribution of internal flexibility of biopolymers is illustrated dramatically by the variability of mean-squared displacements measured in the X-ray diffraction experiment for side-chain and backbone atoms in different portions of the Mb molecule.[12-14]

According to static X-ray structures, the packing of most highly folded proteins can be so dense that often the rotation of buried aromatic side chains of phenylalanine (Phe) and tyrosine (Tyr) is quite difficult to envision.[15,16] Yet, early $^1$H NMR studies have shown that even the most constrained residues exhibit reorientation in the time scale of high-field NMR instruments, $\geq 10^3$ s$^{-1}$.[17,18] The rotation or flipping of buried Phe and Tyr rings is believed to be permitted by concerted motions often described as transient

† Current address: Department of Chemistry, Pennsylvania State University, Davey Laboratory, University Park, PA 16082.

(1) Gurd, F. N. R.; Rothgeb, T. M. *Adv. Protein Chem.* **1979**, *33*, 73-165.
(2) Karplus, M.; McCammon, J. A. *CRC Crit. Rev. Biochem.* **1981**, *9*, 293-349.
(3) Debrunner, P. G.; Frauenfelder, H. *Annu. Rev. Phys. Chem.* **1982**, *33*, 283-299.
(4) Woodward, C.; Simon, E.; Tuchsen, E. *Mol. Cell. Biochem.* **1982**, *48*, 135-160.
(5) McCammon, J. A. *Rep. Prog. Phys.* **1984**, *47*, 1-84.
(6) Case, D. A.; Karplus, M. *J. Mol. Biol.* **1979**, *132*, 343-368.
(7) Austin, R. H.; Beeson, K. W.; Einstein, L.; Fraunfelder, H.; Gunsallus, R. C. *Biochemistry* **1975**, *14*, 5355.
(8) Perutz, M. F.; Mathews, F. S. *J. Mol. Biol.* **1966**, *21*, 199-202.
(9) Perutz, M. F.; Fermi, G. In *Haemoglobin and Myoglobin Atlas of Molecular Structures in Biology*; Phillips, D. C., Richards, F. M., Eds.; Oxford University: Oxford, 1986; Vol. 2.
(10) Dickerson, R. E.; Geis, R. *Hemoglobin*; Benjamin/Cummings: Menlo Park, CA, 1983.
(11) Gelin, B. R.; Karplus, M. *Proc. Natl. Acad. Sci. U.S.A.* **1977**, *74*(3), 801-805.
(12) Fraunfelder, H.; Petsko, G. A.; Tsernoglou, D. *Nature (London)* **1979**, *280*, 558-563.
(13) Parak, F.; Fink, P.; Mayo, K. H. *Biophys. Struct. Mech.* **1980**, *6*, 51.

0002-7863/88/1510-4176$01.50/0 

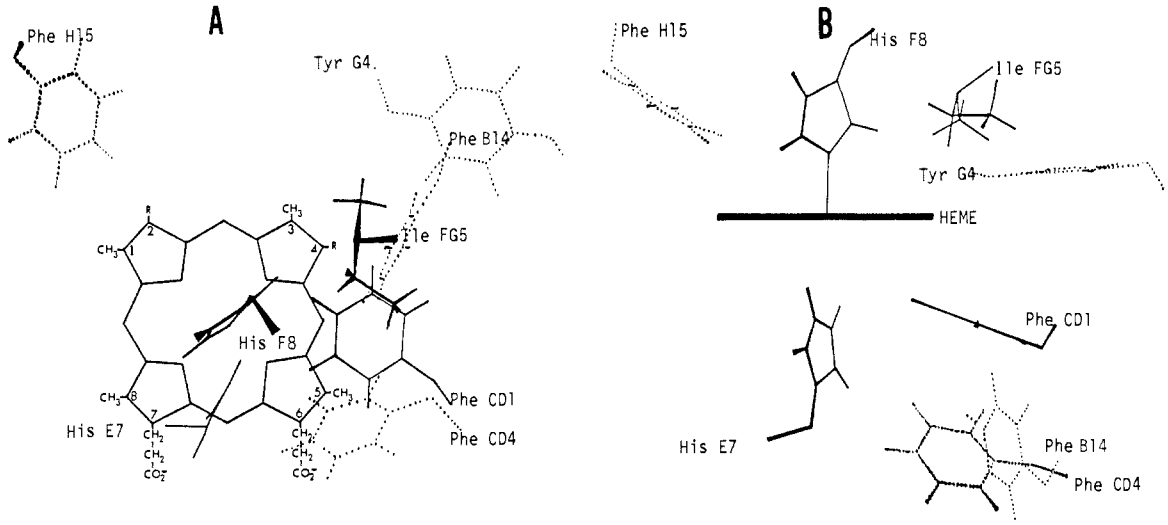


**Figure 1.** Stick diagram showing two orthogonal views of the orientations of selected amino acid side chains with respect to the heme as they occur in the crystal structure of MbCO.[50] Protons are not shown for $\alpha$- and $\beta$-carbons for simplicity. Amino acids are labeled at their $\alpha$-carbons. (A) Porphyrin backbone (R = H for deuterohemin, R = vinyl for protohemin). Proximal residues: His F8, Ile FG5, Tyr G4, Phe H15. Distal residues: Phe B14, Phe CD1, Phe CD4, His E7. (B) Same amino acids shown in A but with an edge-on perspective relative to the heme plane where the 6- and 7-propionate groups of the heme are nearest the viewer.

packing defects. Considerable effort has been expended toward obtaining an understanding of the correlated motions giving rise to such processes.[19-23] While these side-chain motions in themselves may not play any biological role, in some cases the dynamic view of proteins they mirror is relevant to the complete understanding of protein function.

Oxygen-binding heme proteins possess two completely invariant amino acid residues:[24] the proximal His F8, which serves as the axial ligand to the iron, and Phe CD1, which is approximately parallel to and in van der Waals contact with the heme $\pi$ system on the distal side of the heme (see Figure 1). His F8 and Phe CD1 thus provide probes whose dynamic characterization will provide comparative data for related heme proteins. Isotope exchange of the His F8 ring-labile proton and F helix peptide protons have provided qualitative characterization of the flexibility of the proximal heme pocket in a variety of proteins.[25-30] On the other hand, Phe CD1 is packed against the heme and was once visualized as the archetypically immobilized aromatic ring whose interaction with the heme $\pi$ system modulates ligand-binding properties.[31] Recently, both regional variations in mean-square displacements,[32] as well as anisotropic thermal expansion in single crystals of Mb,[33] suggest that the CD corner is more flexible than other regions of the molecule. Moreover, high-field $^1H$ NMR analysis of sperm whale MbCO has revealed that many aromatic amino acids, including Phe CD1, are motionally averaged on the NMR time scale.[34] However, since only completely rotationally averaged Phe CD1 signals could be detected in this protein form, only a lower limit to the reorientation rate could be estimated. In order to use this reorientation rate as a probe of differential flexibility in the CD corner of genetic variants of Mb or Hb, it will be necessary to determine these rates of reorientation in a variety of proteins and, ideally, to obtain the activation energies of this process. Both the reorientation rate and the activation energy will serve as important experimental criteria for assessing computer modeling of the protein dynamics.[32]

Our interest here is in the determination of motional properties of Phe CD1 in a paramagnetic state of Mb. The paramagnetic state of choice is low-spin ferric Met-MbCN, whose sizable magnetic anisotropy[35] imparts large and spatially discriminating dipolar shifts to amino acid side chains in the heme pocket,[36] while still retaining excellent spectral resolution. None of the Phe CD1 resonances have been assigned to date. However, we have recently located the magnetic susceptability axes of met-MbCN, which allow quantitative mapping of the paramagnetic dipolar field.[37] Calculation of both paramagnetic dipolar[38] and ring current[39] shifts

(14) Gelin, B. R.; Lee, A. W.; Karplus, M. *J. Mol. Biol.* **1983**, *171*, 489-559.
(15) Huber, R.; Kukla, D.; Ruhlmann, A.; Steigemann, W. *Cold Spring Harbor Symp. Quant. Biol.* **1971**, *36*, 141-150.
(16) Deisenhofer, J. O.; Steigemann, W. *Acta Crystallogr., Sect. B: Struct. Crystallogr. Cryst. Chem.* **1975**, *B31*, 238-250.
(17) Wagner, G.; De Marco, A.; Wuthrich, K. *Biophys. Struct. Mech.* **1976**, *2*, 139. Wuhrich, K.; Wagner, G. *FEBS Lett.* **1975**, *50*, 265-268.
(18) Wagner, G.; Wuthrich, K.; Tschesche, H. *Eur. J. Biochem.* **1978**, *86*, 67-76.
(19) McCammon, J. A.; Lee, C. Y.; Northrup, S. H. *J. Am. Chem. Soc.* **1983**, *105*, 2232-2237.
(20) Cooper, A. *Proc. Natl. Acad. Sci. U.S.A.* **1976**, *73*, 2740.
(21) Richards, F. M. *Carlsberg Res. Commun.* **1979**, *44*, 47.
(22) Wagner, G. *FEBS Lett.* **1980**, *112*, 280.
(23) Hatzel, R.; Wuthrich, K.; Deisenhofer, J.; Huber, R. *Biophys. Struct. Mech.* **1976**, *2*, 159-180.
(24) Bashford, D.; Chothia, C.; Lesk, A. M. *J. Mol. Biol.* **1987**, *196*, 199-216.
(25) Englander, S. W.; Kallenbach, N. R. *Q. Rev. Biophys.* **1984**, *16*, 521-655.
(26) Ohe, M.; Kajita, A. *Biochemistry* **1980**, *19*, 4443-4450.
(27) Lecomte, J. T. J.; La Mar, G. N. *Biochemistry* **1985**, *24*, 7388-7395.
(28) La Mar, G. N.; Cutnell, J. D.; Kong, S. B. *Biophys. J.* **1981**, *34*, 217-226.
(29) Jue, T.; La Mar, G. N.; Han, K.; Yamamoto, Y. *Biophys. J.* **1984**, *46*, 117-120.
(30) La Mar, G. N.; Krishnamoorthi, R. *Biophys. J.* **1983**, *44*, 177-183.
(31) Rousseau, D. L.; Shelnutt, J. A.; Ondrias, M. R.; Friedman, J. M.; Henry, E. R.; Simon, S. R. *Hemoglobin and Oxygen Binding*; Elsevier: North-Holland: New York, 1982.
(32) Levy, R. M.; Sheridan, R. P.; Keepers, J. W.; Dubey, G. S.; Swaminathan, S.; Karplus, M. *Biophys. J.* **1985**, *48*, 509-518.
(33) Frauenfelder, H.; Hartmann, H.; Karplus, M.; Kuntz, S. D., Jr.; Kuriyan, J.; Parak, F.; Petsko, G. A.; Ringe, D.; Tilton, R. J., Jr.; Connolly, M. L.; Max, N. *Biochemistry* **1987**, *26*, 254-261.
(34) Mabbutt, B. C.; Wright, P. E. *Biochim. Biophys. Acta* **1985**, *832*, 175-185. Dalvit, C.; Wright, P. E. *J. Mol. Biol.* **1987**, *194*, 313-327.
(35) Horrocks, W. DeW., Jr.; Greenberg, E. S. *Biochim. Biophys. Acta* **1973**, *322*, 38-44.
(36) Shulman, R. G.; Glarum, S. H.; Karplus, M. *J. Mol. Biol.* **1971**, *57*, 93.
(37) Emerson, S. D.; La Mar, G. N., manuscript in preparation.
(38) For remotely coordinated amino acid protons in the heme pocket $\delta_{para}$ can be calculated from the dipolar shift equation: $\delta_{para} = (1/2Nr^3)[(\chi_{zz} - \bar{\chi})(1 - 3\cos^2\theta) + (\chi_{yy} - \chi_{xx})(\sin^2\theta \cos 2\Omega)]$, where $N$ is Avogadro's number and $r$, $\theta$, and $\Omega$ are spherical polar coordinates of the proton relative to the principle axes of the magnetic susceptibity tensor $\chi$. $\chi_{xx}$, $\chi_{yy}$, and $\chi_{zz}$ are the reported principle components of $\chi$[35] and $\bar{\chi} = {}^1/_3(\chi_{xx} + \chi_{yy} + \chi_{zz})$. In order to choose the orientation of $\chi$ that best predicts the observed shifts in met-MbCN, a least-squares fit was performed to minimize the error between observed and calculated paramagnetic shifts of assigned resonances. The procedure is completely analogous to that reported for cytochrome *c*. Williams, G.; Clayden, N. J.; Moore, G. R.; Williams, R. J. P. *J. Mol. Biol.* **1985**, *183*, 447-460. Emerson, S. D.; La Mar, G. N., manuscript in preparation.
(39) Cross, K. J.; Wright, P. E. *J. Magn. Reson.* **1985**, *64*, 220-231.

indicates that the *m*- H atoms of Phe CD1[40] are separated by 5.6 ± 1.2 ppm at 25 °C. This large chemical shift difference expected for nonequivalent *m*-H protons could allow quantitation of reasonably rapid ring rotation.

Although the extra chemical shift dispersion provided by interaction with the unpaired electron is useful for expanding the NMR time scale, the large hyperfine shifts and accelerated paramagnetic relaxation prohibit us from taking advantage of conventional diamagnetic chemical shift and spin multiplet patterns for assignment of heme pocket resonances. However, the electron–nuclear dipolar interactions experienced by protons in the heme pocket impart a characteristic temperature dependence to the resonance position that can often be used to recover information about the spin system type (aliphatic, aromatic, etc.). The accelerated paramagnetic relaxation rates, which tend to obscure multiplicities and reduce the magnitude of nuclear Overhauser effects (NOEs),[41] also compensate for this information loss by providing iron–proton distances. Isotope labeling of heme protons has led to clear identification of many resonances originating from the prosthetic group.[42-45] Given these assignments, the observation of NOEs combined with paramagnetic relaxation rates[46] leads to spatial localization of a spin system with respect to the heme periphery and to the iron center.[47,48] Crystal structure data show four phenylalanines (B14, CD1, CD4, H15) and one tyrosine (G4) in close proximity to the heme prosthetic group in sperm whale myoglobin[49-51] (see Figure 1). Of these five aromatic residues, the Phe CD1 side-chain protons are the closest to the iron center and thus are expected to experience the largest perturbations to their resonance positions and their relaxation properties.

## Experimental Section

**Preparation of Samples.** Sperm whale myoglobin was purchased from Sigma Chemical Co. as a lyophilized powder and used without further purification. Cyanometmyoglobin, met-MbCN, was prepared by dissolution of the lyophylate in $^2H_2O$–0.2 M NaCl–20 mM KCN. The pH* of all samples was adjusted with 0.2 M solutions of $NaO^2H$ and $^2HCl$; reported pH* values are uncorrected for isotope effect. NOE data were recorded on approximately 0.5 mL of 5 mM met-MbCN. For the reconstitution with deuterohemin, sperm whale apomyoglobin was prepared according to the reported procedure.[52] A 1.5 mM sample of apomyoglobin in 0.1 M phosphate, pH 7, was reconstituted with 15 mM dicyanodeuterohemin in 0.1 M NaOH. The sample was purified on a Sephadex G25 column and the met-aquo form of the protein was eluted. The solvent was then exchanged with $^2H_2O$–0.2 M NaCl in the ultrafiltration cell. The sample was allowed to stand at room temperature for 3 days in the met-aquo form at pH 9 to achieve equilibration of the heme orientation and labile proton exchange. All samples were ultrafiltered to replace the solvent with fresh $^2H_2O$–0.2 M NaCl–20 mM KCN after labile proton exchange.

**$^1$H NMR Measurements.** $^1$H NMR spectra were recorded on Nicolet NT-360 and NT-500 spectrometers operating in the quadrature mode at 360 and 500 MHz, respectively. Spectra were recorded at the temperature that best resolves the signal of interest. Data were collected using double precision on 16 384 data points over an approximately 30-kHz bandwidth at 500 MHz. Typical spectra consisted of at least 1280 transients with a repetition rate of 1.2 $s^{-1}$. Chemical shifts for all the spectra are referenced to 2,2-dimethyl-2-silapentane-5-sulfonate, DSS, through the residual water resonance.

The selective $T_1$ of signal e was measured by inversion recovery at 500 MHz. The decoupler was used to generate the selective pulse. Recovery data were analyzed with a three-parameter nonlinear least-squares fit. For the case of dominant electron–nuclear dipolar relaxation, the nuclear $T_{1i}$ is proportional to the sixth power of the iron–proton distance, $R_i$. Thus, the use of $T_{1j}$ for a signal whose protons are a known distance from the iron, $R_j$, along with the measurement of $T_{1i}$ provides a means of calculating $R_i$ through eq 1.[47]

$$T_{1i}/T_{1j} = (R_i/R_j)^6 \quad (1)$$

Homonuclear decoupling data were collected with a 13-kHz spectral window on the 360-MHz spectrometer. Gated decoupler power was applied during acquisition with the decoupler on-resonance. Corresponding reference spectra were collected under identical conditions but with the decoupler pulse off-resonance. On- and off-resonance frequencies were alternated every 96 scans.

The steady-state nuclear Overhauser spectra were recorded at 500 MHz by application of a presaturation pulse of 250 ms with the decoupler on-resonance with off-resonance spectra collected to provide a reference. Truncated NOE data were collected in an analogous way except the decoupler presaturation pulse duration was varied. Computer difference spectra were generated to quantitate the fractional intensity change $\eta$, which can be related to the cross-relaxation rate $\sigma$ and the selective relaxation rate $\rho$ through eq 2,[41] where $i$ and $j$ are two protons

$$\eta_{ij}(t) = \frac{I_i^j - I_i^0}{I_j^0} = \frac{\sigma_{ij}}{\rho_j}[1 - \exp(-\rho_j t)] \quad (2)$$

interacting through the dipolar relaxation mechanism. For short irradiation times ($t$) the change in $\eta_{ij}$ with time has been shown to be linearly related to the cross-relaxation rate (eq 3).[53] The cross-relaxation rate,

$$(d\eta_{ij}/dt)_{t\to 0} = -\sigma_{ij} \quad (3)$$

$\sigma_{ij}$, for rigid molecules tumbling slowly in solution is given by eq 4,[54]

$$\sigma_{ij} = -\gamma^4\hbar^2\tau_c/10r_{ij}^6 \quad (4)$$

where $r_{ij}$ is the interproton separation and $\tau_c$ is the correlation time for molecular reorientation. For long irradiation times and in the absence of spin diffusion,[55] eq 2 reduces to the steady-state NOE (eq 5).[56] Thus,

$$\eta_{ij} = \sigma_{ij}/\rho_j \quad (5)$$

the steady-state NOE does not yield distance information unless $\rho_j$ is obtainable, and hence its use in obtaining $\sigma_{ij}$ is restricted to resolved resonances. However, such NOEs can still be used to establish proximity. In cases in which an NOE is observed to a proton $j$ from two different protons $i$ and $k$, the relative distances $r_{ij}$ and $r_{jk}$ can be estimated even without knowledge of $\rho_j$. The present system of interest, met-MbCN, exhibits completely negligible spin diffusion within the needed irradiation times.

**Determination of Dipolar Shifts.** The observed chemical shift of a proton in met-MbCN ($\delta_{total}$) can be regarded as the sum of diamagnetic and paramagnetic terms:

$$\delta_{total} = \delta_{peptide} + \delta_{ring\ current} + \delta_{para} \quad (6)$$

$\delta_{peptide}$ is the reported tetrapeptide shift,[57] $\delta_{ring\ current}$ is obtained from ring current calculations[39] on the $MbO_2$ crystal structure,[49] and $\delta_{para}$ is calculated from the paramagnetic dipolar shift equation.[38]

## Results and Discussion

The low-field portions of the resolved 500-MHz spectra of met-MbCN in $^2H_2O$ at a series of temperatures are illustrated in Figure 2. The upfield region of the 45 °C spectrum is included in Figure 3A. Peaks a, c, and f have been assigned to heme 5-$CH_3$, 1-$CH_3$, and 8-$CH_3$, respectively, through isotope labeling

(40) We have chosen to use the notation for ring protons of Phe in which the two protons attached to δ-carbons (in the crystallographic notation) ortho to the β-methylene group are referred to as *o*-H, the meta protons (bonded to ε-carbons) are *m*-H, and the para proton (bonded to the ζ-carbon) is the *p*-H.

(41) Noggle, J. H.; Shirmer, R. E. *The Nuclear Overhauser Effect*; Academic: New York, 1971.

(42) Mayer, A.; Ogawa, S.; Shulman, R. G.; Yamane, T.; Cavaleiro, J. A. S.; RochaGonsalves, A. M. d'A.; Kenner, G. W.; Smith, K. M. *J. Mol. Biol.* **1974**, *86*, 749–756.

(43) La Mar, G. N.; Davis, N. L.; Parish, D. W.; Smith, K. M. *J. Mol. Biol.* **1983**, *168*, 887–896.

(44) La Mar, G. N.; Emerson, S. D.; Lecomte, J. T. J.; Pande, U.; Smith, K. M.; Craig, G. W.; Kehres, L. A. *J. Am. Chem. Soc.* **1986**, *108*, 5568–5573.

(45) Shulman, R. G.; Wuthrich, K.; Yamane, T.; Antonini, E.; Brunori, M. *Proc. Natl. Acad. Sci. U.S.A.* **1969**, *63*, 623–628.

(46) La Mar, G. N.; Horrocks, W. DeW., Jr.; Holm, R. H. *NMR of Paramagnetic Molecules: Principles and Applications*; Academic: New York, 1973.

(47) Cutnell, J. D.; La Mar, G. N.; Kong, S. B. *J. Am. Chem. Soc.* **1981**, *103*, 3567–3572.

(48) Lecomte, J. T. J.; La Mar, G. N. *Eur. Biophys. J.* **1986**, *13*, 373–382.

(49) Phillips, S. E. V. *J. Mol. Biol.* **1980**, *142*, 531–554.

(50) Hanson, J. C.; Shoenborn, B. P. *J. Mol. Biol.* **1981**, *153*, 117–146.

(51) Takano, T. *J. Mol. Biol.* **1977**, *110*, 537–568.

(52) Teale, F. W. J. *Biochim. Biophys. Acta* **1959**, *35*, 543.

(53) Wagner, G.; Wuthrich, K. *J. Magn. Reson.* **1979**, *33*, 675.

(54) Solomon, I. *Phys. Rev.* **1955**, *90*, 559.

(55) Kalk, A.; Berendsen, J. J. C. *J. Magn. Reson.* **1976**, *24*, 343–366.

(56) Dobson, C. M.; Olejniczak, E. T.; Poulsen, F. M.; Ratcliffe, R. G. *J. Magn. Res.* **1982**, *48*, 97–110.

(57) Bundi, A.; Wuthrich, K. *Biopolymers* **1979**, *18*, 285–297.

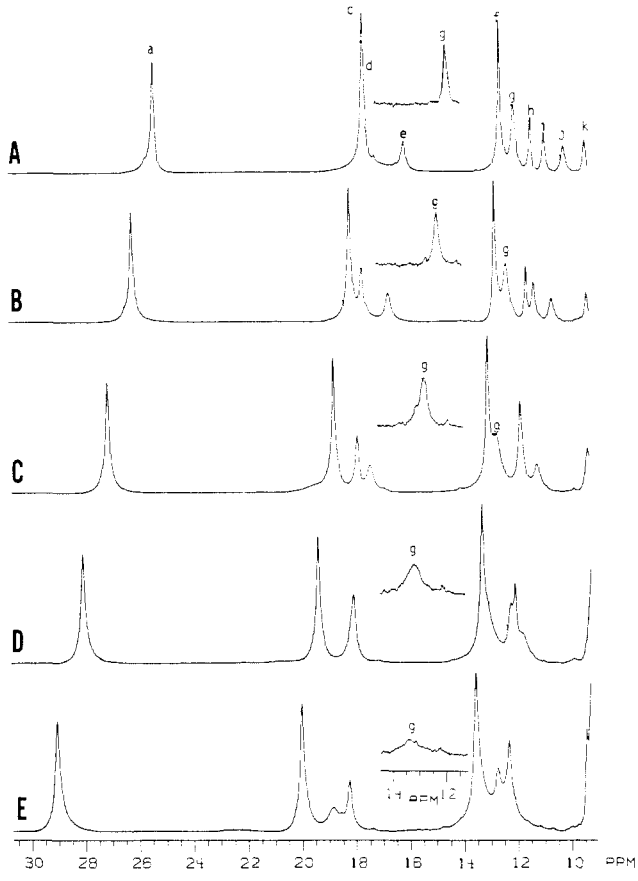


**Figure 2.** Downfield regions of the 500-MHz $^1H$ NMR spectra for a 5 mM solution of met-MbCN in $^2H_2O$, pH 8.6, at various temperatures: (A) 45 °C, (B) 35 °C, (C) 25 °C, (D) 15 °C, (E) 5 °C. Insets in A–E show a portion of the NOE difference spectrum obtained upon presaturation of signal e (see text), allowing visualization of the line shape of signal g at temperatures where it is not resolved from the 8-$CH_3$ (signal f).

of the heme;[42,43] peaks d, h, and i have been assigned to the heme 2-vinyl $C^{\alpha}H$, distal His E7 $C^{\delta}H$, and proximal His F8 $C^{\beta}H$, respectively, on the basis of NOE studies.[48] Resolved upfield signals identified in previous NOE studies include peaks v, w, x, and z, whose respective assignments are heme 2-vinyl $C^{\beta}H$ (trans to $C^{\alpha}H$)[58] and Ile FG5 $C^{\gamma}H_3$, $C^{\delta}H_3$, and $C^{\gamma'}H$.[59] Resolved signals unassigned to date are the single proton peaks e, j, k, and u and the peak g.

Experimental data illustrated in Figure 2 show that signal g, when resolved (>40 °C), integrates to two-proton intensity and appears to remain a single resonance at all temperatures. Moreover, when compared with the other resolved resonances, it exhibits anomalous line broadening as the temperature is lowered. Since it is unlikely that two hyperfine shifted signals would remain accidentally degenerate over such a wide temperature range, and since the peak broadens at lower temperature, we explore the hypothesis that g results from the rapid motional averaging of two protons, such as the two *o*-H or the two *m*-H of a phenyl or tyrosine ring. We demonstrate in the following section that signal g indeed arises from motionally averaged *m*-H of a Phe and that its nearest neighbors clearly identify it as Phe CD1.

**Steady-State NOEs.** Figure 3A illustrates the 500-MHz $^1H$ NMR spectrum of met-MbCN in $^2H_2O$ at 45 °C and pH 8.7. The experimental conditions were selected to optimize resolution of g, the signal of interest. The NOE difference trace resulting from the saturation of peak g is shown in Figure 3B. An NOE

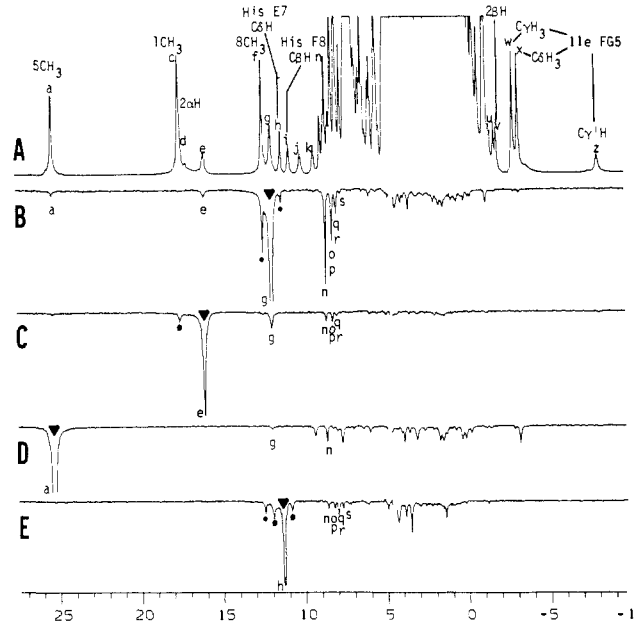


**Figure 3.** 500-MHz $^1H$ NMR spectra of met-MbCN in $^2H_2O$, pH 8.7 45 °C. (A) Reference spectrum with previously assigned heme signals (a = 5-$CH_3$, c = 1-$CH_3$, d = 2-vinyl $C^{\alpha}H$, f = 8-$CH_3$, v = 2-vinyl $C^{\beta}H_{trans}$) and previously assigned amino acid signals (h = His E7 $C_4H$, i = His F8 $C^{\beta}H$. Ile FG5 signals: w = $C^{\gamma}H_3$, x = $C^{\delta}H_3$, z = $C^{\gamma}H$) labeled in the spectrum. The intense diamagnetic and aromatic envelopes have been truncated. (B–E) NOE difference spectra obtained upon saturation at the frequency indicated by the arrow. Black dots indicate decoupler spillage to neighboring resonances.

of −3.1 ± 0.6% is detected to the resolved single proton peak e, as well as NOEs to numerous peaks in the unresolved envelope. The selective $T_1$ of peak e is 19 ± 2 ms (see below). Thus, eq 5 yields $\sigma_{ge} = -1.6 \pm 0.4$ s$^{-1}$, which together with the known molecular reorientation time of 8 ns for Mb at 45 °C[48,60] yields $r_{ge} = 2.6 \pm 0.2$ Å through use of eq 4. The NOE between g and e is consistent with their origin as neighboring protons on an aromatic ring,[61] which indicates that e is due to *p*-H and g is due to the averaged two *m*-H of a Phe, ruling out the Tyr. This demands that saturation of g should yield large NOEs to each of the two Phe *o*-H signals. Since the difference in the two *o*-H shifts is predicted[37,38] to be smaller than the difference in the two *m*-H shifts, it is expected that the two *o*-H signals are also motionally averaged. Figure 3B reveals a very strong NOE to peak n at 8.5 ppm (and weaker NOEs to other peaks in the 7.5–8.0 ppm window; see below), making this peak a leading candidate for the averaged *o*-H signal.

**Spin–Spin Coupling.** The coupling constant between vicinal partners on a phenyl ring is known to be approximately 7–8 Hz. The assignment of e, g, and n to the spin system of a Phe ring implies that such coupling should be observed between g (*m*-H) and n (*o*-H) and between g (*m*-H) and e (*p*-H). The coupling to the *p*-H (e) is not expected to be resolved owing to the efficient relaxation of that signal[62] ($T_1^{-1} \approx 50$ Hz > 2 J). The g–n spin–spin interaction, however, may be observable. Figure 4A presents an expanded portion of the downfield hyperfine shifted region of the spectrum containing peaks g and n. Figure 4B is the NOE difference trace obtained upon saturation of g, showing clearly the location of resonance n. The difference spectrum generated in the homonuclear spin–spin decoupling experiment is illustrated in Figure 4C: on-acquisition irradiation of g causes a typical

(58) Ramaprasad, S.; Johnson, R. D.; La Mar, G. N. *J. Am. Chem. Soc.* **1984**, *106*, 3632–3635.
(59) Ramaprasad, S.; Johnson, R. D.; La Mar, G. N. *J. Am. Chem. Soc.* **1984**, *106*, 5330–5335.
(60) Marshall, A. G.; Lee, K. M.; Martin, P. W. *J. Am. Chem. Soc.* **1980**, *102*, 1460–1462.
(61) The model used to calculate the NOE assumes that both protons of signal g contribute equally to the observed intensity change for signal e. If one assumes that the entire effect comes from only one of the two protons of g, the $\sigma = -3.2$ s$^{-1}$ leads to $r_{ge} = 2.3$ Å, which is slightly less than the van der Waals distance between two protons not attached to the same carbon.
(62) Frankel, L. S. *J. Chem. Phys.* **1969**, *50*, 943–950.

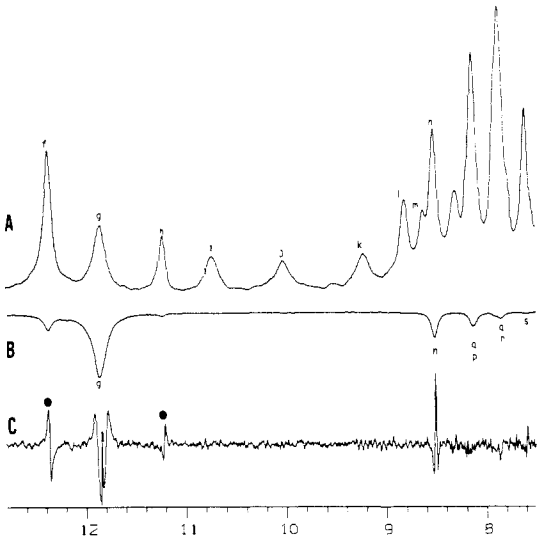


**Figure 4.** (A) Downfield portion of the 360-MHz $^1$H NMR spectrum for the same sample as in Figure 3. (B) Downfield region of Figure 3B showing the position of the NOEs from signal g. (C) Difference spectrum obtained by subtracting the data shown in Figure 4A from a spectrum in which decoupler power was applied to g during acquisition. Note the dispersion signals as expected by the Bloch-Siegert shift are labeled with a dot.

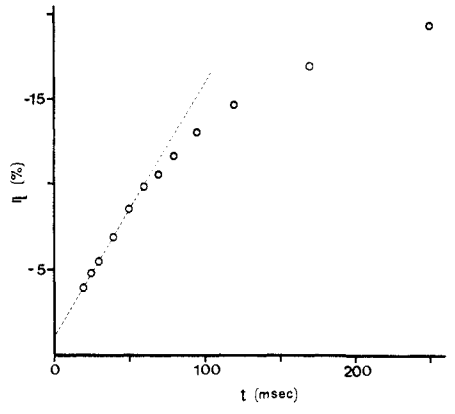


**Figure 5.** Time dependence of $\eta$ when signal n at 8.5 ppm is observed for varying saturation times $t$ of signal g. The dotted line illustrates the least-squares line through the initial data points with $t$ in the range 20–60 ms having the equation $\eta_{gn}(t) = -1.5t - 0.02$.

sharpening of the same resonance n. This establishes the through-bond connectivity between n and g.

**Time-Dependent NOEs.** Since the selective $T_1$ for peak n cannot be determined directly, we turn to the time-dependent NOE to obtain $\sigma_{gn}$, and thus $r_{gn}$. The buildup of the NOE to n upon saturating g is illustrated in Figure 5. The least-squares fit of the initial slope yields $\sigma_{gn} = -1.5$ s$^{-1}$.[53] The use of eq 4 with $\tau_c = 8$ ns again yields $r_{gn} = 2.6 \pm 0.1$ Å, which is completely consistent with the *o*-H to *m*-H distance of a Phe ring. It should be noted that ring reorientation does not influence the *m*-H to *o*-H NOE since this vector is parallel to the axis about which such motion occurs.[63] For the steady-state $\eta_{ge}$, ring reorientation will not lead to a decrease of the NOE as long as the reorientation rate is much slower than the bulk rotational correlation time[63] (which will be shown to be the case). Thus, both the NOE and spin-decoupling data concur in assigning the e, g, n set of resonances to a Phe ring that is reorienting fast on the NMR time scale.

**Spin–Lattice Relaxation.** Signal *e* has a very short $T_1$, 19 ± 2 ms, indicating a strong interaction with the unpaired spin of the iron. Using the 8-$CH_3$, $T_{1f} = 150 \pm 20$ ms, $R_f = 6.20 \pm 0.03$ Å, and $T_{1e} = 19 \pm 2$ ms in eq 1, yields $R_e = 4.4 \pm 0.1$ Å. The

(63) London, R. E. *J. Am. Chem. Soc.* **1978**, *100*, 2678–2685.

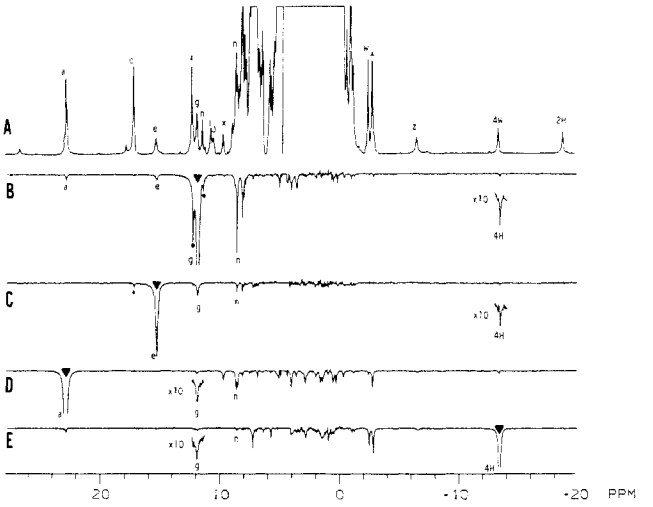


**Figure 6.** 500-MHz $^1$H NMR spectra of deuterohemin-reconstituted met-MbCN in $^2H_2O$, pH 8.7, 45 °C. (A) Reference spectrum. Signals have been labeled such that isostructural resonances are given the same label in both Figures 3 and 6. (B–E) NOE difference spectra obtained upon saturation at the frequency indicated by the arrow. Black dots indicate decoupler spillage to neighboring resonances. Note the similarities between Figures 6B–D and 3B–D demonstrating the same dipolar connectivities in the native protein.

X-ray crystal structures of MbCO[50] and $MbO_2$[49] place the *p*-H of the Phe CD1 at 4.3 and 4.5 Å, respectively, from the iron. Earlier NOE studies in $H_2O$ have already established that signal g originates from the distal side of the heme.[48] Thus, signal e must also be of distal origin, ruling out the possibility that e, g, and n come from Phe H15, on the proximal side of the heme.

**Spatial Localization of Phe CD1.** Figure 3B shows that a small NOE is seen from g to the heme 5-$CH_3$ (peak a). Saturation of the 5-$CH_3$ yields NOEs to both g and n, as seen in Figure 3D. Single-crystal structural data illustrated in Figure 1[50] show Phe CD1 to be located between the 4- and 5-positions of the heme. Unfortunately, none of the 4-vinyl protons are resolved in the spectrum of met-MbCN, and consequently proximity of the e–g–n spins to that position of the heme is difficult to establish in the native protein. Thus, we turn to deuterohemin-reconstituted met-MbCN (Figure 1A, R = H). Previous studies of this reconstituted protein in solution[64,65] have demonstrated that the deuterohemin orientation is the same as that for the native protohemin (Figure 1A, R = vinyl). Figure 6A illustrates the $^1$H NMR spectrum of deuterohemin–met-MbCN. Isotope labeling of the heme has provided assignment of the heme methyls;[64] steady-state NOE studies have also identified the deuterohemin 2-H and 4-H signals, as well as the signals of Ile FG5.[65] The cleanly resolved 4-H signal is a convenient probe of the heme environment near the 4-position.

Comparison of the $^1$H NMR spectra of native met-MbCN (Figure 3A) and deuterohemin–met-MbCN (Figure 6A) confirms the strong similarities in their molecular/electronic structures and NMR spectral parameters. Repeating the native protein NOE experiments of Figure 3B–D with deuterohemin–met-MbCN yields the analogous difference traces illustrated in Figure 6B–D. Virtually indistinguishable NOE patterns are observed in the two proteins when the same residue is irradiated, further supporting the conserved structure in spite of modification of the 2,4-substituents. Thus, the NOE data in Figure 6B–D argue that peaks e, g, and n arise from the same Phe resonances in both native and deuterohemin-reconstituted proteins. Moreover, Figure 6B shows that saturation of g yields an NOE not only to signal e, the 5-$CH_3$

(64) La Mar, G. N.; Budd, D. L.; Viscio, D. B.; Smith, K. M.; Langry, K. C. *Proc. Natl. Acad. Sci. U.S.A.* **1978**, *75*, 5755–5759.
(65) Johnson, R. D.; Ramaprasad, S.; La Mar, G. N. *J. Am. Chem. Soc.* **1983**, *105*, 7205–7206.
(66) Kaplan, J. I.; Fraenkel, G. *NMR of Chemically Exchanging Systems*; Academic: New York, 1980; p 78.

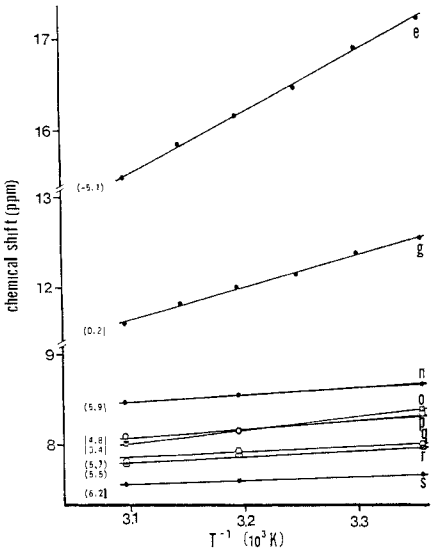


**Figure 7.** Temperature dependence of chemical shift for signals e, g, and the signals in the aromatic region that show NOEs from g. Numbers in parentheses are intercepts of the best fit line through the data points.

(signal a), and some aromatic signals but also to the 4-H resonance at −13.5 ppm. Saturation of the 4-H peak yields small NOEs to n and g, as shown in Figure 6E. Comparison of parts D and E of Figure 6 (D, NOE obtained from 5-$CH_3$; E, NOE obtained from 4-H) determines that signal n corresponds to protons that are closer to the 5-$CH_3$ than the 4-H, while g is roughly equidistant from the 4- and 5-positions of the heme. Thus, geometrical arrangement of proton e and the two proton pairs giving rise to peaks g and n is completely consistent with Phe CD1 being in the same average orientation in solution as in the X-ray structure of MbCO and $MbO_2$ (Figure 1).

**Other Phenylalanines.** Figure 3B shows that, in addition to the large NOE to n, two other NOEs can clearly be seen in the 8.3–7 ppm region. Repeating the NOE experiment at different temperatures shows that these signals at 8.1 and 7.9 ppm are actually pairs of NOEs that are nearly degenerate at 45 °C. Figure 7 shows the results of the variable-temperature NOE experiments in which signal g was saturated. The chemical shift of the resonances experiencing the NOE, as well as that of g, are plotted vs inverse temperature (Curie plot). For each trace, the number in parentheses gives the extrapolated intercept of the chemical shift at infinite temperature. The paramagnetic shift varies primarily as the inverse temperature;[46] thus, ideally the extrapolation to infinite temperature should give the diamagnetic chemical shift. However, the signals experiencing strong dipolar shifts, such as e and g, have extrapolated intercepts that overshoot their diamagnetic values; this effect is due to the contribution of paramagnetic shift terms quadratic in the inverse temperature.[46] On the other hand, less shifted signals extrapolate more closely to their expected diamagnetic chemical shifts. Five of the signals that show NOE from g extrapolate to a diamagnetic intercept in the aromatic region (5–8 ppm). One of these signals is signal n, the *o*-H of Phe CD1; the others are as yet unassigned. The insensitivity of the shifts for peaks p–s to changes in temperature indicates that the paramagnetic contributions to their total chemical shifts are very small. The 5–8 ppm shifts of these signals suggest that they originate from aromatic ring protons. Examination of the crystal structure data (Figure 1) shows two other Phe residues in the vicinity of Phe CD1: Phe B14 and Phe CD4. Although the variability of the relative orientations of these three side chains in reported crystal structures[49-51] precludes an unambiguous assignment of the signals to individual protons, the distances are such that the aromatic NOEs seen from g are likely to come from these two residues. The fact that saturation of His E7 $C^{\delta}H$ (shown in Figure 3E) also yields these NOEs further supports their origin as Phe B14 and Phe CD4; however, the assignments of peaks p–s should be regarded as tentative.

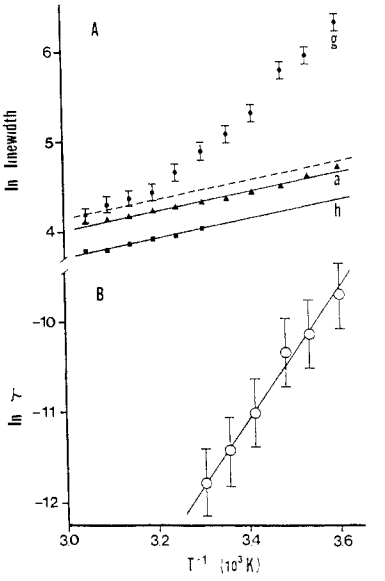


**Figure 8.** (A) Natural log of the line width of signals a, h, and g for the sample described in Figure 2 as a function of inverse absolute temperature. Parallel lines correspond to the temperature dependence of line width in the absence of exchange. The dotted line is the extrapolated line width behavior expected for signal g in the absence of any exchange contribution. (B) Natural log of the state lifetime for Phe CD1 ring rotation $\tau$ as a function of inverse absolute temperature.

**Phe CD1 Reorientation.** The observation that the two-proton signal g assigned to the motionally averaged *m*-H broadens anomalously as the temperature is lowered (Figure 2) indicates that the exchange of the two nonequivalent *m*-H sites makes a detectable contribution to the observed line widths. Characterization of signal g below 25 °C at pH 8.6 is difficult because of the serious overlap of peaks g and f. However, accurate determination of the line width of g can be obtained at any temperature via analysis of NOE difference traces from signal e as shown in the insets of Figure 2. Line width data obtained in this way are plotted vs inverse temperature in Figure 8A.

It is not possible to "freeze" out the Phe CD1 rotation in the slow-motion limit even at 0 °C and 500 MHz. Since the conventional line shape analysis in both slow- and fast-motion limits is not possible, we must extract the kinetic parameters for ring rotation solely from the exchange contribution to the line shape of the motionally averaged signal. In the applicable regime of rapid exchange, the collapsed resonance exhibits an exchange contribution to the line width, $\Delta\nu_{ex}$, given by the eq 7,[66] where

$$\Delta\nu_{ex}^{i}(T) = (\pi/4)[\Delta\delta_i(T)]^2\,\tau(T) \qquad (7)$$

$\Delta\delta_i$ is the chemical shift difference in the absence of exchange (in frequency units) and $\tau$ is the reorientation time of the phenyl ring, both of which depend on temperature $T$. Qualitative support for the exchange origin of the observed signal broadening is provided by the fact that signal g shows appreciable line narrowing at 360 MHz relative to 500 MHz (not shown) as predicted for the $\Delta\delta_i$ term in eq 7.

A quantitative estimate of $\tau$ in eq 7 can be made when $\Delta\nu_{ex}^{g}$ and $\Delta\delta_g$ are determined. The $\Delta\nu_{ex}^{g}$ term is obtained from the plot of ln line width vs reciprocal temperature shown in Figure 8A. In the absence of exchange, this plot yields a series of parallel lines,[67] as shown for signals a (heme 5-$CH_3$) and h (His E7 $C^{\delta}H$). At temperatures above 40 °C, peak g shows negligible exchange contribution to its line width. The deviation of the g line widths at lower temperatures over the extrapolated high-temperature value (dotted line) yields $\Delta\nu_{ex}^{g}$ of 61 ± 9 Hz at 25 °C and 500 MHz.

$\Delta\delta_g$ is obtained from eq 6 where $MbO_2$ X-ray coordinates[49] provide the structural data from which both ring current and

(67) La Mar, G. N.; Van Helke, G. R. *J. Chem. Phys.* **1970**, *52*, 5676–5681.

paramagnetic dipolar shifts are calculated for the individual protons of the Phe CD1 ring.[38] Addition of these shifts to the tetrapeptide shift[57] for Phe ring protons yields the predicted resonance positions for the "frozen" Phe CD1 ring. At 25 °C, the calculated chemical shifts are 8.7 and 14.3 ppm (average 11.3 ppm) for the two *m*-H, 8.6 and 7.8 ppm (average 8.2 ppm) for the two *o*-H, and 17.1 ppm for the unique *p*-H, which correspond closely to the observed rotationally averaged shifts at 12.6, 8.7, and 17.3 ppm, respectively. The $\Delta\delta_{m\text{-}H}$ of 2.8 ± 0.6 kHz at 500 MHz leads to a state lifetime for two-site exchange $\tau = 10 \pm 4$ μs at 25 °C through eq 7. Casting $\tau(T) = \tau_0 \exp(-E_a/RT)$, where $E_a$ is the activation barrier to reorientation and assuming that the two individual *m*-H resonances exhibit the same temperature dependence as found for the mean shift (Figure 7) lead to a straight line for the plot $\tau(T)$ versus $T^{-1}$ (Figure 8B) with a slope that yields $E_a = 14 \pm 4$ kcal/mol.

Thus, we have determined the reorientation rate of phenyl ring rotation $\sim 10^5$ Hz at 25 °C and made an estimate of $E_a$ (14 kcal/mol) for Phe CD1 in one state of Mb.[68] This activation energy is well below the reported denaturation enthalpy of 40 kcal/mol[69] for metMb at pH 9 and 25 °C and hence rules out global unfolding. Its value is closer to the range of activation barriers reported for the conformational changes associated with solvent penetration in BPTI (0-15 kcal/mol)[70] and hence is consistent with concerted motions within the folded protein allowing the ring flips.[19] A preliminary survey of Mb genetic variants in the met-cyano state indicates that, while the chemical shift of a resonance with the same NOE connectivities as peak g (averaged *m*-H) is very similar, both its highly variable line width and temperature sensitivity suggest variations in phenyl ring reorientation. It is thus likely that the definitive assignment and detailed elucidation of the exchange properties of such resonances will provide at least one index of the relative flexibility of the C-D corner in Mb and Hb. Detailed studies of such genetic variants, including the use of cryosolvents to freeze out the Phe CD1 motion, are in progress.

**Acknowledgment.** This research was supported by a grant from the National Science Foundation (CHE-84-15329). S.D.E. was supported by NIH Training Grant in Molecular and Cellular Biology GM07377.

**Registry No.** L-Phe, 63-91-2.

(68) It has been reported that the 2-D NMR assigned *m*-H peaks of sperm whale MbCO are motionally averaged.[34] Assuming the kinetics are the same in both MbCO and MbCN, estimation of $\Delta\delta_{m\text{-}H} = 2.6 \pm 0.3$ ppm based on ring current calculations[39] and the *m*-H coordinates of the "frozen" Phe CD1 in the crystal structure of MbCO,[50] $MbO_2$,[49] and met-Mb[51] leads to $\Delta\nu_{ex} = 12 \pm 4$ Hz at 25 °C and 50 ± 20 Hz at 10 °C for SwMbCO at 500 MHz. Thus exchange broadening should be observable for MbCO at low temperatures unless the reorientation rate of the Phe CD1 side chain is faster in MbCO than in met-MbCN.

(69) Hermans, J., Jr.; Acampora, G. *J. Am. Chem. Soc.* **1967**, *89*, 1547-1552.

(70) Woodward, C. K.; Hilton, B. D. *Biophys. J.* **1980**, *10*, 561-575.

# Atomic and Group Electronegativities from the Electron Density Distributions of Molecules

**Russell J. Boyd* and Kenneth E. Edgecombe**

*Contribution from the Department of Chemistry, Dalhousie University, Halifax, Nova Scotia B3H 4J3, Canada.* *Received June 24, 1987*

**Abstract:** The topological properties of the electron density distributions of molecules are used to define a method for the evaluation of atomic and group electronegativities. According to the bond critical point model, the electronegativity of an atom relative to hydrogen is calculated from properties associated with the bond critical point of the corresponding diatomic hydride. Atomic electronegativities of the 21 main-group elements from lithium to bromine are shown to correlate with atomic electronegativities based on empirical and nonempirical methods. A straightforward extension of the method is used to obtain the electronegativities of 30 groups from the electron density distributions of polyatomic molecules. The group electronegativities are shown to correlate with values from a variety of methods, the exceptions being methods based on total electronegativity equalization. A potential advantage of the bond critical point method is the possibility of direct evaluation of group electronegativities from experimental electron density distributions.

The concept of electronegativity is frequently traced to the work of Pauling[1] in the 1930s. Not only is Pauling's definition of electronegativity as "the power of an atom in a molecule to attract electrons to itself" regarded as the classical definition, but his numerical scale, based on thermochemical data, has been used extensively for qualitative and quantitative discussions. Phillips[2] claims, however, that the concept of relative electronegativity arose in the 18th century in connection with oxidation-reduction potentials. Binary compounds of atoms with large differences in electronegativity were observed by early crystallographers to form rock salt structures while smaller differences in electronegativity lead to more open covalent structures. In any case, electronegativity is very much a part of the vocabulary of contemporary chemistry.

Numerical electronegativity scales have established two general trends: Electronegativity increases from left to right within a given row of the periodic table of the elements and decreases from top to bottom. Moreover, innumerable correlations between electronegativity values and various physical and chemical properties have played a central role in the organization and rationalization of chemical facts and observations.

Electronegativity scales belong to one of two classes. In the empirical methods, thermochemical data, ionization energies and electron affinities, dipole moments, internuclear distances in crystals, atomic spectral data, parameters from magnetic resonance spectra, or other properties are used to assign an electronegativity

(1) Pauling, L. *The Nature of the Chemical Bond*, 3rd ed.; Cornell University: Ithaca, NY, 1960, and references therein.

(2) Phillips, J. C. *Rev. Mod. Phys.* **1970**, *42*, 317-356.

0002-7863/88/1510-4182$01.50/0 